

# The MJO and global warming: a study in CCSM4

Aneesh Subramanian · Markus Jochum ·  
Arthur J. Miller · Richard Neale · Hyodae Seo ·  
Duane Waliser · Raghu Murtugudde

Received: 11 December 2012 / Accepted: 13 June 2013 / Published online: 27 June 2013  
© Springer-Verlag Berlin Heidelberg 2013

**Abstract** The change in Madden–Julian oscillation (MJO) amplitude and variance in response to anthropogenic climate change is assessed in the 1° nominal resolution community climate system model, version 4 (CCSM4), which has a reasonable representation of the MJO characteristics both dynamically and statistically. The twentieth century CCSM4 run is compared with the warmest twenty-first century projection (representative concentration pathway 8.5, or RCP8.5). The last 20 years of each simulation are compared in their MJO characteristics, including spatial variance distributions of winds, precipitation and outgoing longwave radiation, histograms of event amplitude, phase and duration, and composite

maps of phases. The RCP8.5 run exhibits increased variance in intraseasonal precipitation, larger-amplitude MJO events, stronger MJO rainfall in the central and eastern tropical Pacific, and a greater frequency of MJO occurrence for phases corresponding to enhanced rainfall in the Indian Ocean sector. These features are consistent with the concept of an increased magnitude for the hydrological cycle under greenhouse warming conditions. Conversely, the number of active MJO days decreases and fewer weak MJO events occur in the future climate state. These results motivate further study of these changes since tropical rainfall variability plays such an important role in the region's socio-economic well being.

**Keywords** MJO · Climate change · CCSM4

---

A. Subramanian (✉) · A. J. Miller  
SIO, UCSD, La Jolla, CA 92037, USA  
e-mail: acsubram@ucsd.edu

M. Jochum  
Climate and Geophysics Division, The Niels Bohr Institute,  
Copenhagen, Denmark

R. Neale  
Climate and Global Dynamics Division, National  
Center for Atmospheric Research, Boulder, CO, USA

H. Seo  
Physical Oceanography Department, Woods Hole  
Oceanographic Institution, Woods Hole, MA, USA

D. Waliser  
Jet Propulsion Laboratory, California Institute of Technology,  
Pasadena, CA, USA

R. Murtugudde  
Earth System Science Interdisciplinary Center,  
University of Maryland, College Park, MD, USA

## 1 Introduction

The Madden–Julian oscillation (MJO) is the dominant tropical intraseasonal pattern in the earth's climate system (Madden and Julian 1994; Zhang 2005; Lau and Waliser 2012). The MJO has been shown to impact the variability of the monsoon systems (Lau and Waliser 2012; Waliser 2006), to interact with El Niño/Southern oscillation events (McPhaden 1999; Zhang and Gottschalck 2002; Lau 2005), and affect deep oceanic variability (Matthews 2004; Matthews et al. 2007). Long-term changes in MJO statistics have been observed in the historical climate record by Jones and Carvalho (2006). This may indicate that changes in the background conditions can influence MJO properties (also see Zhou et al. 2012b). Future climate scenarios simulated with the global coupled model ECHAM4 (Liu et al. 2012) reveal that the MJO tends to amplify under conditions associated with global warming. Yet other

aspects of the MJO behavior, such as changes in regional structure, frequency of occurrence, and magnitude of events, have not been studied extensively in this global warming context.

Here we examine changes in the MJO in the community climate system model, version 4 (CCSM4) for an extreme climate change scenario for the twenty-first century. CCSM4 has a reasonable representation of the MJO characteristics both dynamically and statistically, as shown by Subramanian et al. (2011) for a pre-industrial control run of CCSM4. The focus here is on analyzing the changes to the structure and amplitude of the MJO in a global warming scenario compared to a twentieth century simulation. By comparing standardized measures of MJO responses (Waliser et al. 2008), these two runs can be compared to estimate the impact of a changed climate due to greenhouse gas forcing on this important tropical mode of variability.

While improvements in simulating MJO dynamics have occurred over the years, global climate models still do not realistically reproduce all characteristics of the observed MJO (Zhang 2005; Lin et al. 2006). The objective of this study is to show projections of possible changes in the activity of the MJO under one particular extreme climate warming scenario for one model that simulates the MJO well. Understanding the MJO response to global warming is likely to be most pronounced under this extreme scenario. Although there remains considerable uncertainty concerning the magnitude of the global climatic temperature response to a given increase in greenhouse gases, a number of climatic responses are tightly coupled to the temperature response (Held and Soden 2006; Meehl et al. 2012). Most of these are related, directly or indirectly, to lower-tropospheric water vapor. Since previous studies indicate that lower-tropospheric water vapor will increase as the climate warms (Seager et al. 2012; O’Gorman and Schneider 2009b; Held and Soden 2006; Trenberth et al. 2003; Allen and Ingram 2002), key phenomena that are intimately tied to the hydrological cycle, like MJO, will likely be modified by this increase in water vapor. The results found here indeed indicate that important changes do occur in the intensity and spatial structures of MJO activity.

Section 2 briefly describes the CCSM-4 model, the observational data sets, and the methodology used to diagnose the MJO and changes related to global warming. Section 3 describes the changes in the mean climate of the Tropics due to global warming in dynamical and hydrological fields. Section 4 compares the MJO response in the future climate to that of the twentieth century and the main changes to the MJO structure and activity in the future climate are described. A summary and discussion are given in Sect. 5.

## 2 Model simulations and methodology

### 2.1 CCSM-4 model

The CCSM4 includes a finite volume dynamical core with a nominal  $1^\circ$  resolution ( $0.9^\circ \times 1.25^\circ$ ), 26 level version of community atmosphere model, version 4 (CAM4). There have been a number of changes to the dynamics and moist physics in CAM4 (Gent et al. 2011, 2010). The finite volume dynamical core (Lin 2004) replaces the spectral Eulerian core as the default dynamical core in CAM4. The deep convection scheme has two key modifications: the calculation of convectively available potential energy (CAPE) is now based on a dilute entraining parcel (Neale et al. 2008), and the sub-grid scale vertical transport of momentum by deep convection is included according to Richter and Rasch (2008). The convection scheme changes provide significant improvements to the mean atmosphere climate of CAM4 (Zhou et al. 2012a), and improvements are even larger when CAM4 is coupled within CCSM4 (Gent et al. 2011). More striking are the improvements to transient climate variability within the tropics, related to higher frequency convectively forced and dynamically coupled variability (Neale et al. 2012). Strong precipitation events are more frequent, the precipitation diurnal cycle is more accurate, and the representation of the MJO (Subramanian et al. 2011; Zhou et al. 2012b) and ENSO (Neale et al. 2008; Deser et al. 2012) is improved. Numerous aspects of the CCSM4 ocean model ( $1^\circ$  resolution, with meridional refinement to  $.25^\circ$  at the equator) have improved as well (Gent et al. 2011), resulting in such things as a sharpening of the equatorial currents and a more realistic representation of tropical instability waves (Jochum et al. 2008).

Analysis here focuses on the CCSM4 simulations carried out for the coupled model intercomparison project (CMIP5). We analyzed a current climate CCSM4 experiment, which includes a combination of anthropogenic and natural forcings representative of the twentieth century (Gent et al. 2011). The anthropogenic forcings include time-evolving GHGs, and also prescribed concentrations of tropospheric ozone, stratospheric ozone, the direct effect of sulfate aerosols and black and primary organic carbon aerosols that evolve spatially and temporally.

Representative concentration pathways (RCPs) runs of CCSM4 are also available (Lamarque et al. 2010, 2011; Meehl et al. 2012). These provide a profile of radiative forcing, derived using specified socio-economic models (Moss et al. 2010). We analyze the RCP8.5 case, which changes the globally averaged top-of-atmosphere radiative balance by  $8.5 \text{ W/m}^2$ . This run bears on the extreme climate change scenario, which is most likely to show a strong signal in changes to the MJO. For this analysis, we consider the 20-year time periods of 1981–2000 and

2081–2100 for comparison. We first discuss the changes to the mean SST and tropical atmospheric circulation pertinent to changes in MJO in the following section, and then address changes in MJO itself in subsequent sections.

### 2.2 Methodology

The time series of variables from the CCSM4 model for the twentieth century run and the twenty-first century run are saved as daily mean values for analysis. The anomalies for the winds, precipitation and outgoing longwave radiation (OLR) for the last 20 years of each run are computed after removing the climatological mean for the last 20 year period of the respective centuries. The anomaly fields are then filtered with a 20–100 day band pass filter to isolate the MJO signal. The variance, wavenumber-frequency power spectra and differences thereof for the two centuries are computed. A multivariate EOF analysis (Wheeler and Hendon 2004) is then performed on the zonal winds at 850 and 200 hPa and OLR to derive the first two linear modes of variability in the tropics, which explain about 40 % of the variance. The differences in the MJO fields thus identified are then illustrated with further analysis of the principle components of these EOFs and the spatial distribution of the EOFs. Histograms of MJO activity, defined as days during which MJO amplitude exceeds a certain threshold (1.0 or 1.5, as specified in Table 1) for at least 10 consecutive days, and MJO phase, defined as number of days the MJO is active in four regions around the global tropics, are also used to diagnose changes. Composite maps of the MJO evolution for the two 20 year periods are also computed based on the MJO index derived from the first two PCs of the EOF analysis (as explained in Waliser et al. 2008).

### 3 Changes to mean climate and its variance

Changes in SST in these two CCSM-4 runs were previously described by Stevenson et al. (2011). SST increases

throughout the tropics, with the east–west gradient of SST along the equatorial Pacific decreasing in the eastern tropics and increasing in the western tropics as seen in Fig. 1. Overall, the mean east–west SST difference, computed as area-averaged SST in the east and west equatorial Pacific Ocean as described in Karnauskas et al. (2009), decreases from roughly 4.2° in the twentieth century to 3.8° in the twenty-first century.

As Tokinaga et al. (2012) suggest, coincident changes in the Walker Cell may occur with these SST gradient changes. We computed their measure of Walker Cell change, which is based on equatorial zonal gradients of area averages of sea level pressure (SLP) and SST. The result for this pair of runs,  $\delta(\text{SST}) = -0.4 \text{ K}/60 \text{ yr}$ ,  $\delta(\text{SLP}) = +0.03 \text{ hPa}/60 \text{ yr}$ , does not suggest any strong change in the Walker Cell has occurred (and falls on their Fig. 3 graph near the values for the twentieth century reanalysis).

To further identify possible changes in the vertical structure of the equatorial atmospheric circulation, Fig. 2 shows the 850mb winds for current climate along with the change in the twenty-first century. A strengthening of both the westerlies over the Maritime Continent (MC) and the easterlies in the central equatorial Pacific occurs in the mean state for the twenty-first century, resulting in stronger convergence in the western equatorial Pacific. Vertical velocity at 500 mb in the twenty-first century case (Fig. 3) also increases between the MC and the dateline, suggesting a local intensification of the updraft branch of the Walker Cell in that region. At 200 mb in the twenty-first century (Fig. 2), stronger divergence occurs in that region as well. Taken together, stronger convergence near the surface and stronger divergence aloft are linked by air rising more vigorously in the western equatorial Pacific. This region, however, is much further east of the area where the strongest rising air occurs over the MC in the mean twentieth century climate.

In the eastern tropical Pacific, the picture is less clear. Easterly winds at 850 mb decrease, which reduces

**Table 1** Difference in number of MJO active days (defined as days with MJO amplitude >1.5 for the table above and >1.0 for the table below) in CCSM4, [RCP8.5 (twenty-first century) – (twentieth century)]

	Western Hemisphere	Indian Ocean	Maritime Continent	West Pacific
Days (twenty-first – twentieth century) (%)	12 ± 8	32 ± 12	14 ± 8	31 ± 12
Mean amplitude diff. (%)	7	4	8	3
Days (twenty-first – twentieth century) (%)	3 ± 4	11 ± 8	−4 ± 4	3 ± 4
Mean amplitude diff. (%)	7	4	7	3

Confidence intervals represent 5 % significance levels based on a two-sided *t* test using the relation for standard error for histograms,  $SD = N_k - N_k^2/N$ , (where  $N_k$  is the sample size in each bin) by (D’Agostini 2003) and each 16 days is assumed to be one independent sample. The number of degrees of freedom was computed using a lag-1 autocorrelation. The difference in mean amplitude (RCP8.5—twentieth century) is indicated on the bottom row of the table. Confidence intervals represent 5 % significance levels based on a two-sided *t* test using the standard deviations of the amplitudes and assuming each day is an independent sample. The change in amplitude is always positive indicating that the average amplitude of the MJO is increasing in the future climate

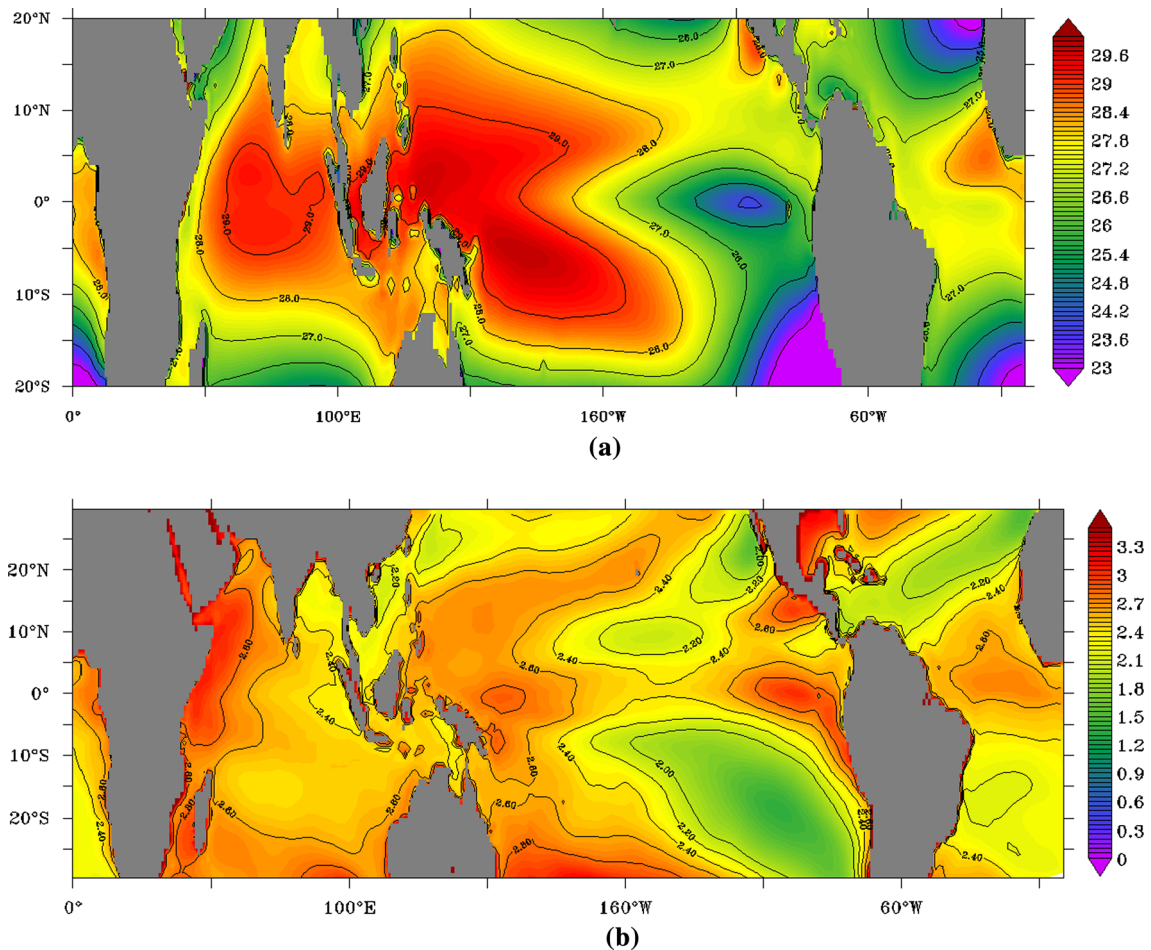


**Fig. 1** Annual mean surface temperature ( $^{\circ}\text{K}$ ) for **a** the twentieth century forcing, **b** difference between the twenty-first and twentieth century. The period used to calculate for were the last 20 years from each century

equatorial upwelling and contributes to warming the SST in that region. Westerly winds aloft at 200 mb are reduced and vertical velocity at 500 mb decreases. A simple local relation between divergence and convergence of the tropical wind fields and vertical velocity is not evident in the simulations. Over the Indian Ocean (IO), where SST has warmed in the twenty-first century run, the vertical velocity at 500 mb decreases, as does the shear in the 200–850 mb zonal wind fields.

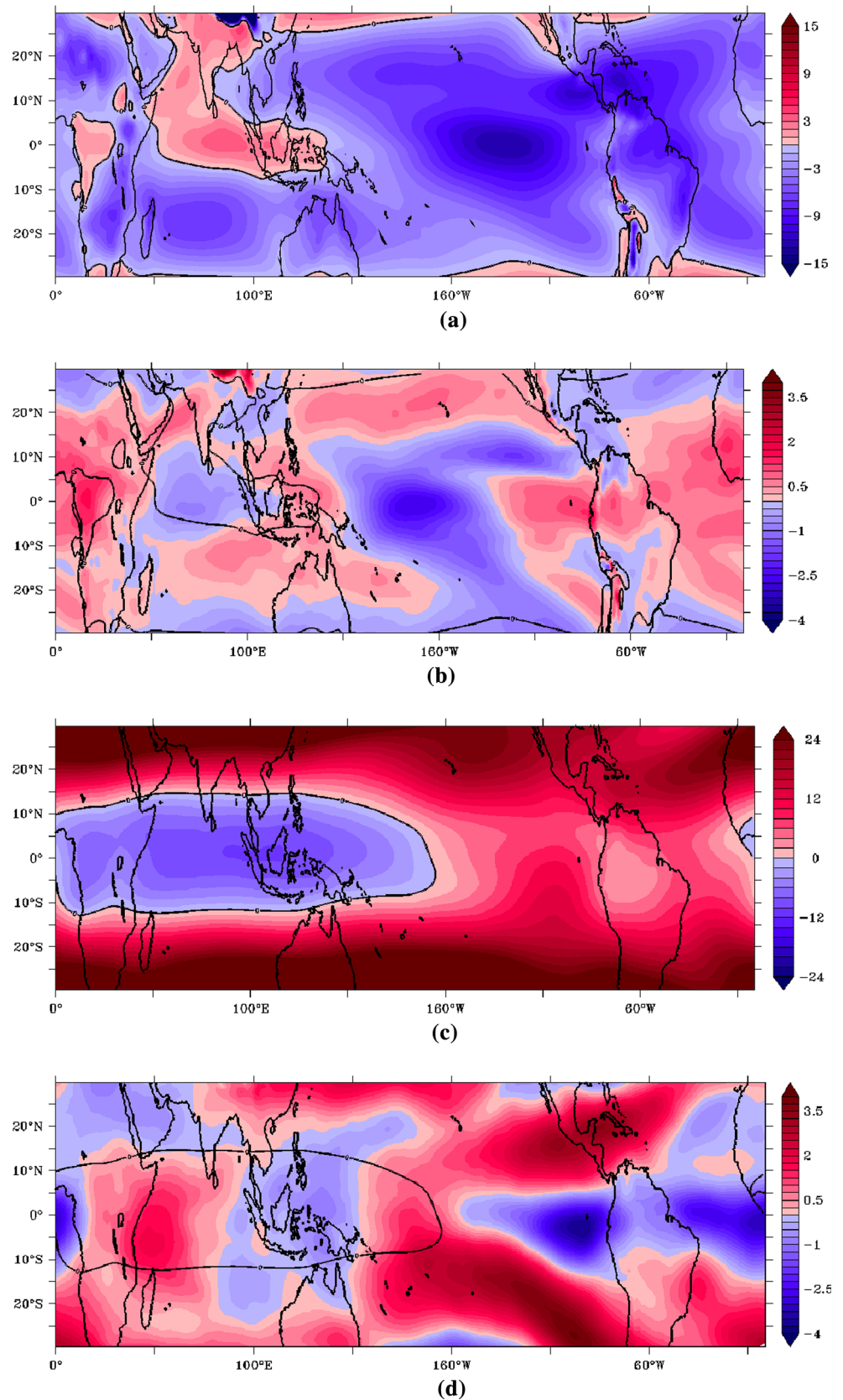
While the mean OLR pattern shown in Fig. 4 generally mimics the mean SST pattern in the twentieth century run, the change in OLR does not exhibit the same east–west structure along the equator as the change in SST for twenty-first century conditions. Instead, it has a large change towards cloudier conditions over the warm pool, where SST rises moderately, and weak change over the eastern tropical Pacific, where SST warms strongly. The lack of a strong change in the eastern tropical Pacific OLR may be due to the low background convection in this region.

Previous studies suggest that the atmospheric Walker Cell in the tropics should weaken in response to climate change (Vecchi et al. 2006; Held and Soden 2006) due to an imbalance between increases in the evaporative flux and convective precipitation. But that adjustment process does not seem to apply here where much more complicated processes occur. The connection between the SST zonal gradients and the overlying Walker Cell perturbation (e.g., Tokinaga et al. 2012) in the twenty-first century run is not obvious and does not appear to directly relate to the results of Vecchi et al. (2006) and Held and Soden (2006).

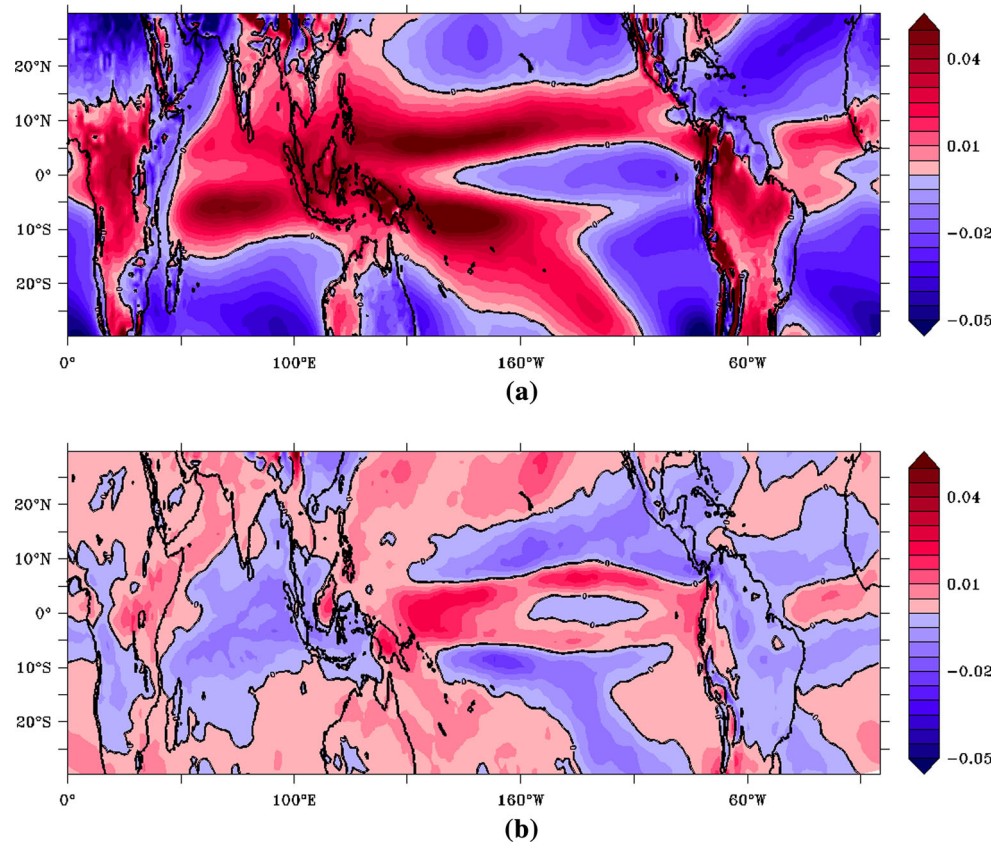
#### 4 Changes to the MJO

The MJO occurs as an energetic climate mode of intra-seasonal variability in both current climate and future climate scenarios. In order to isolate the fraction of variance associated with intraseasonal oscillations, key fields are bandpassed to 20–100 day periods. Both the total (Fig. 5)

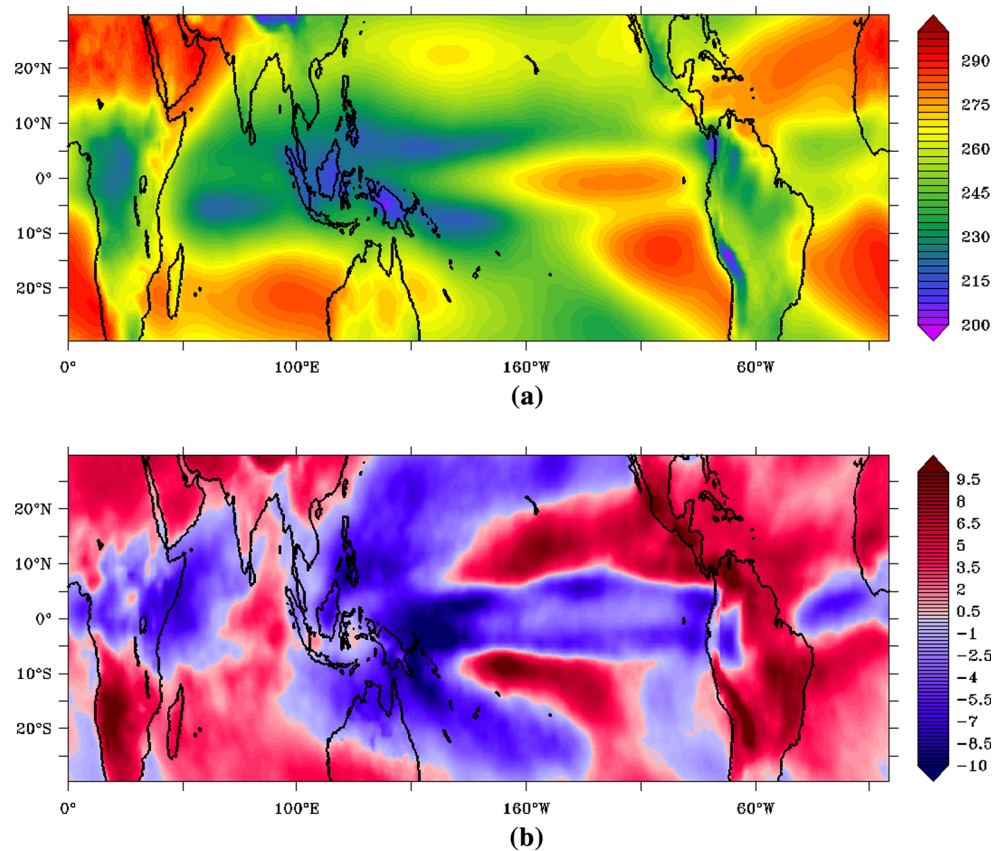
**Fig. 2** **a** Annual mean zonal winds (m/s) at 850 hPa for the twentieth century forcing and **b** the difference between the twenty-first and twentieth century. **c** Annual mean zonal winds at 200 hPa for the twentieth century forcing and **d** the difference between the twenty-first and twentieth century for the same. The period used to calculate for were the last 20 years from each century



**Fig. 3** Annual mean vertical velocity (Pa/s) at 500 hPa for **a** the twentieth century forcing, **b** difference between the twenty-first century and twentieth century. The period used to calculate for were the last 20 years from each century



**Fig. 4** Annual mean OLR ( $W/m^2$ ) for **a** the twentieth century forcing, **b** difference between the twenty-first and twentieth century for the same. The period used to calculate for were the last 20 years from each century



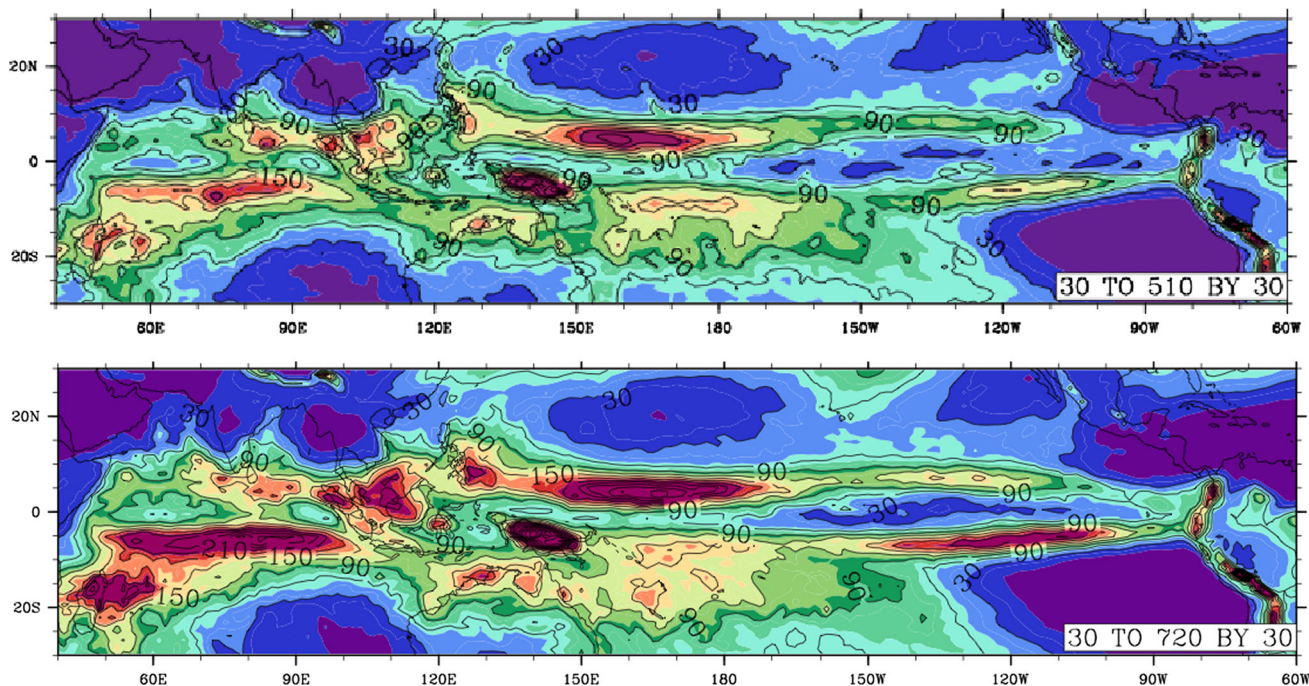


**Fig. 5** Total precipitation variance ( $\text{mm}^2/\text{day}^2$ ) for 50 years of twentieth century (*top*) and twenty-first (*bottom*) simulation

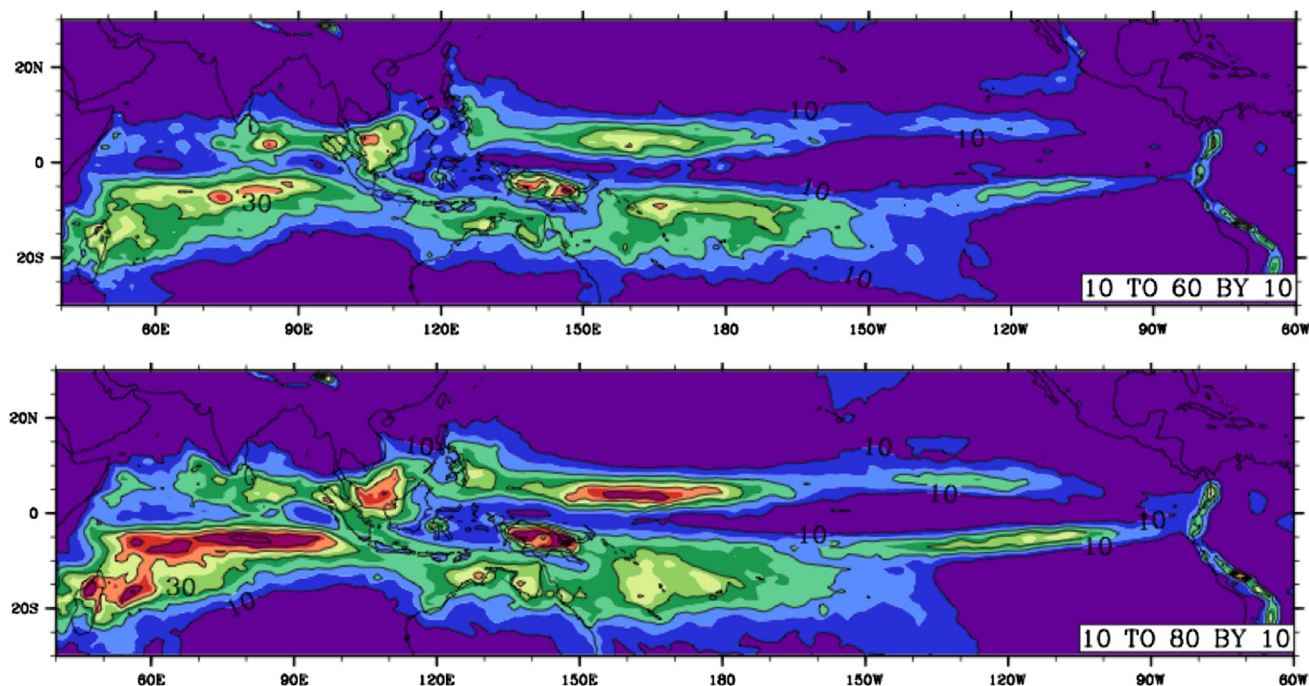


**Fig. 6** Percentage variance of intraseasonal precip in the twentieth century (*top*) and twenty-first century (*bottom*) run. The contours are drawn for every 10 % increase in variance explained by the intraseasonal precipitation

and the intraseasonal (Fig. 6) precipitation variance exhibits a distinct net increase under global warming, while preserving a similar spatial distribution as the current climate case. This is consistent with an amplification of the water cycle in a global warming scenario in CCSM4 which

has been studied earlier in idealized GCMs and climate models (Allan and Soden 2008; Schneider et al. 2010; O’Gorman and Schneider 2008, 2009a). The total variance in the zonal 850 hPa winds (Fig. 7) has the same general pattern for both cases, except for a 10–20 % decrease in the

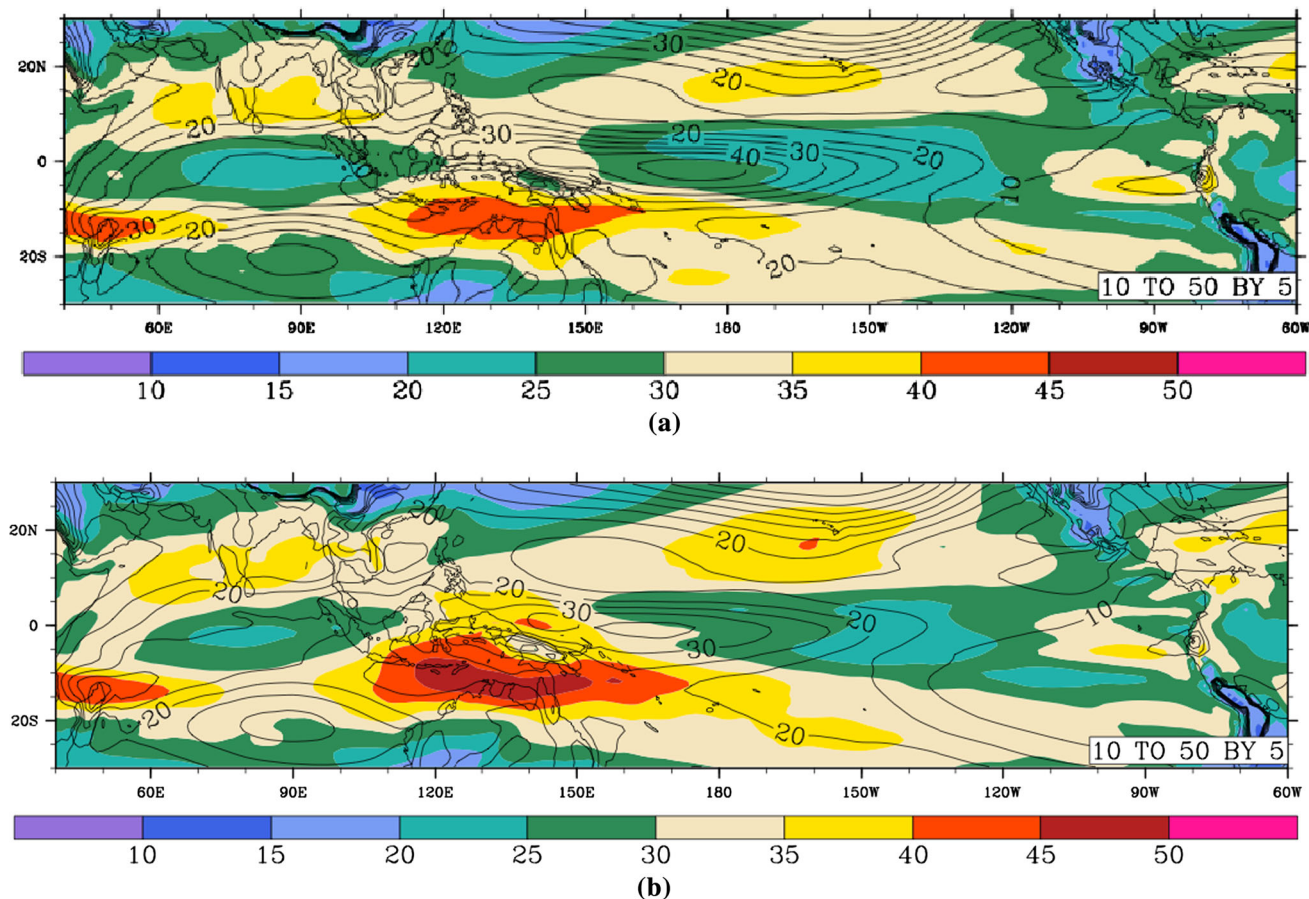


**Fig. 7** Total variance in the zonal 850 hPa winds (line contours, in  $\text{m}^2/\text{s}^2$ ) and percentage variance explained by the intraseasonal oscillations (color contours) for **a** the twentieth century simulation and **b** the twenty-first century simulation

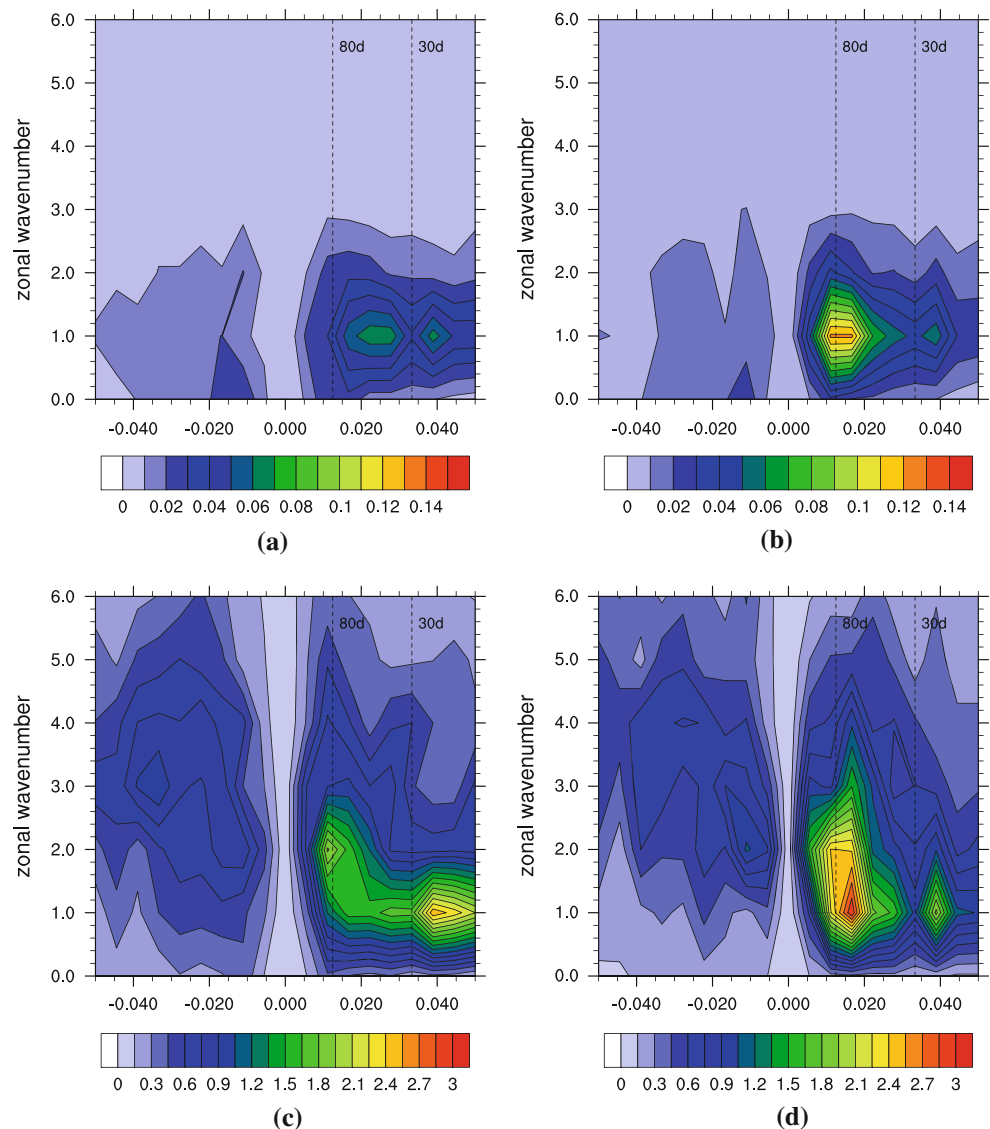
RCP8.5 forced run in the western equatorial Pacific Ocean region. It is unclear from our analysis why the precipitation variance increases in the RCP8.5 forced run while the 850 hPa zonal wind variance decreases in this region. Likewise, the intraseasonal variance in the 850 mb zonal winds explains a similar fraction of total variance, except over the MC, where it explains roughly 10 % more. We next identify MJO spectral changes for these ISOs.

The power spectra for OLR and 850 hPa winds are enhanced in wavenumbers 1–4 (Fig. 8) in the eastward propagation directions indicating an enhanced MJO. There is also increased power in the lower frequencies in the twenty-first century run. The enhanced lower frequency power in winds and convection combined with an increased eastward propagation of the MJO convection indicate a slower, more intense MJO convection propagating eastward in the warmer and wetter Tropics. There is an enhancement at zonal wavenumber one for the 45–120 day periods for the 850 hPa spectra. There is also a substantial enhancement at zonal wavenumber one to three at about 45–120 day periods and slower for the OLR spectra. We next focus on the MJO structural changes.

The MJO Index (MJOI) is diagnosed by computing the combined EOFs of 850, 200 mb winds, and OLR and projecting the spatial patterns onto the total fields. Values of MJOI  $>1.0$  are selected as indicating active MJO days. The CEOFs for each case are shown in Fig. 9. CEOF2 of future climate corresponds to CEOF1 of twentieth century climate and CEOF1 of future climate corresponds to CEOF2 of the twentieth century. The corresponding CEOFs are surprisingly similar for the two different climates, except for a key structural change in OLR across the tropical Pacific in one of the modes (CEOF2 for the future climate case) and a flipping of order in the dominant CEOFs associated with a change in explained variance. In the current climate case CEOF1, the OLR jumps from the nodal point at  $120^\circ\text{E}$  to high values in the western equatorial Pacific and then decreases slowly towards the east. In the future climate case CEOF2, the OLR rises steadily from the nodal point near  $120^\circ\text{E}$  to high values in the eastern equatorial Pacific. This suggests a stronger penetration of MJO rainfall activity across the tropical Pacific in the future climate case.

The frequency of MJOI activity, defined as the number of days when MJOI  $>1$  with a duration of at least 10 days,

**Fig. 8** Wavenumber-frequency power spectra ( $\text{m}^2/\text{s}^2$ ) for 850 hPa zonal winds averaged in the boreal winter seasons over  $10^\circ\text{S}$ – $10^\circ\text{N}$  for **a** the twentieth century forcing and **b** the twenty-first century forcing. Wavenumber-frequency power spectra ( $\text{W}^2/\text{m}^4$ ) for Outgoing Longwave Radiation averaged in the boreal winter seasons over  $10^\circ\text{S}$ – $10^\circ\text{N}$  for **c** the twentieth century forcing and **d** the twenty-first century forcing. The period used to calculate for were the last 20 years from each century



for the twentieth century and the RCP8.5 case is presented in Fig. 10 as a histogram. The number of active MJO days decreases slightly in the global warming scenario as shown by the first point in the histogram difference plot. However, when the MJO is active in the future climate case, the MJO events tend to be of much higher amplitude. There are a greater number of events from  $\text{MJOI} = 3$  to 7 in the global warming case, while the weaker MJO, with  $\text{MJOI} = 1$ – $2$ , become less frequent. The increase in number of days in the RCP8.5 run with MJO amplitude  $>2$  is also consistent with the increase in variance of the intraseasonal precipitation (Fig. 6). These results provide more evidence for an enhanced hydrological cycle in the future climate scenario.

The phases of the CEOF provide another way to identify changes in the spatial structure of MJO activity in the future climate scenario. For example, when the  $\text{MJOI}$  phase is 2 and 3, convection is strong in the IO and

suppressed downstream. So if these phases are more prevalent in one simulation, it indicates regional changes in MJO activity. Using this approach, the number of MJO active days are binned into four phases, each associated with a region: IO (phases 2–3), MC (phases 4–5), West Pacific Ocean (WPO, phases 6–7) and Western Hemisphere (WH, phases 8–1). Table 1 shows the percentage difference in number of strong active days (for  $\text{MJOI} > 1.0$ ) in each regional phase grouping for future climate from current climate. Only the Indian Ocean shows a strong change in this case. Recognizing that strong events are more common in the warmer climate (Fig. 10), we recomputed those statistics for  $\text{MJOI} > 1.5$ . By this criterion, both the IO and WPO show a strong increase, and in addition the MC and WH both show a moderate increase, in MJO activity. The mean amplitude of  $\text{MJOI}$  activity in each phase also increases, the largest change being 0.2 for

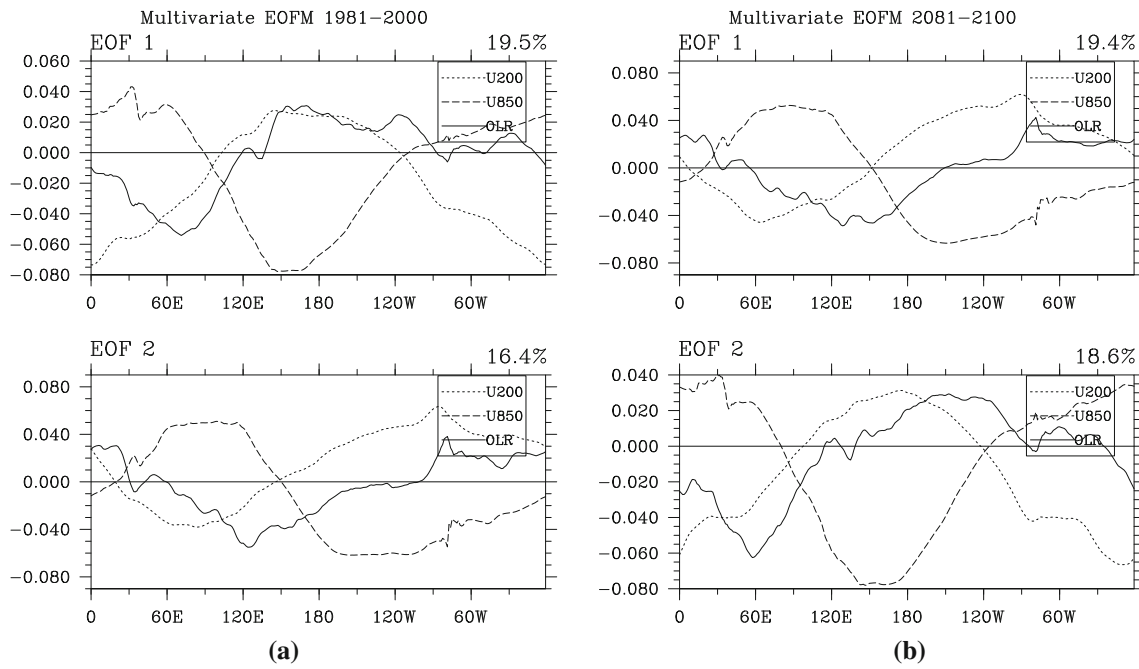


**Fig. 9** Multivariate EOF for zonal winds at 200 and 850 hPa and OLR in the twentieth century (*top*) and twenty-first century (*bottom*) run. **a** Twentieth century, **b** twenty-first century

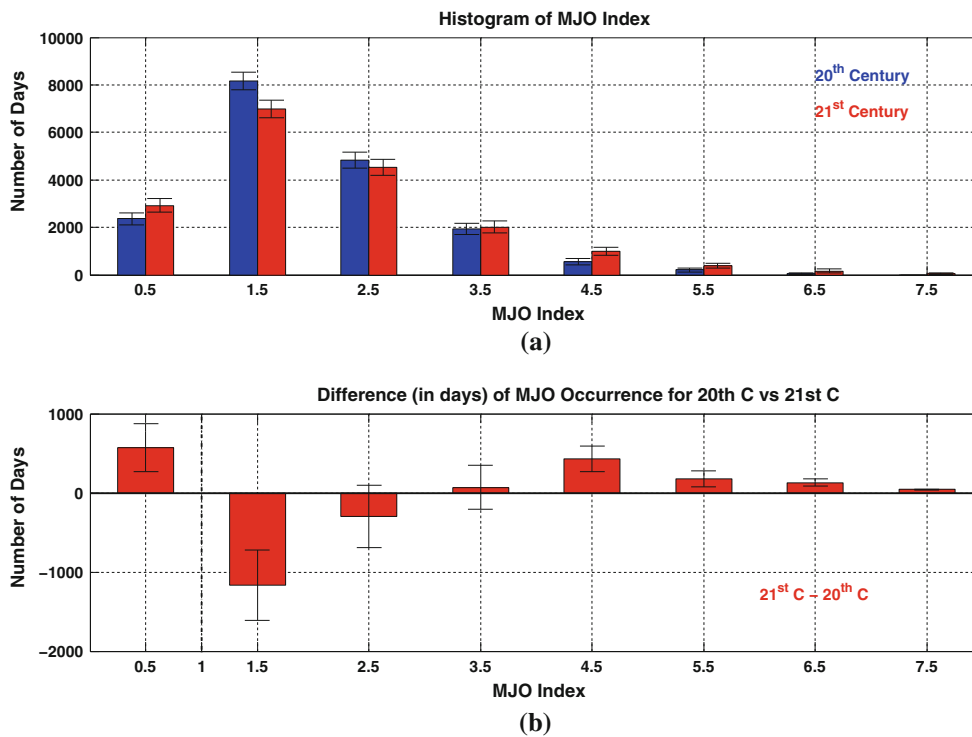


**Fig. 10** MJO activity in the present vs future climate of RCP8.5 scenario. The number of days that the MJO is active at a certain MJO amplitude is plotted as a line histogram in **a**. The difference between the present and future MJO active days for each amplitude is plotted in **b**. Error bars in **a** represent 95 % confidence intervals based on

assuming each 16-day period (from lagged autocorrelation) is an independent sample and using the relation for standard error for histograms  $STD = N_k - N_k^2/N$ , by D’Agostini (2003). Error bars in **b** represent 5 % significance levels based on a two-sided *t* test

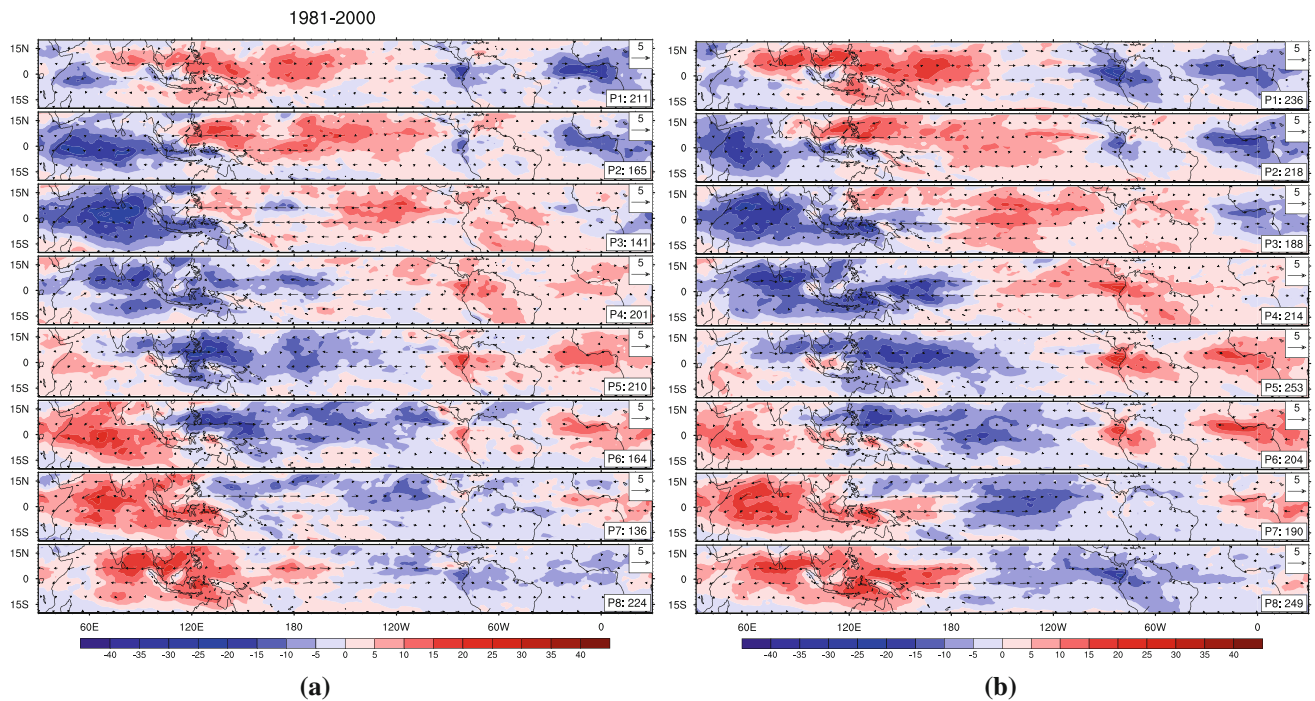


**Fig. 11** Phases of the MJO in winds at 850 hPa (*arrows*, in m/s) and OLR (*color contours*, in  $\text{W/m}^2$ ) for the twentieth century simulation (*left panel*) and the twenty-first century for the same (*right panel*). **a** Twentieth century, **b** twenty-first century

the WH and MC phase, which corresponds to a 7 % increase while the other two regions show an increase of 0.1 in the mean amplitude. This is consistent with the increase in variance of the intraseasonal precipitation observed in the Tropics in the RCP8.5 case.

Figure 11 shows the composite reconstruction of a typical MJO event for both current and the future climate cases. As expected from the previous results, the basic structure of MJO in both cases is very similar. However, one can identify enhancements to the magnitude and structure of OLR activity in two key places. Phases 3, 4 and 5 have a much stronger extension of convective activity across the MC and into the western Pacific. Likewise, phases 6 and 7 have a larger scale and more coherent precipitation structure in the eastern Pacific. Both these effects are consistent with the general warming of SST across the equatorial region and the consequent greater availability of ambient water vapor for general convective systems. Previous studies have shown an increased eastward propagation of the MJO during El Niño events, supported by the warmer waters in the central and eastern Pacific (Roundy et al. 2010; Zhang and Gottschalck 2002). Also, Maloney et al. (2010) show that a reduced meridional SST gradient, such as is found in the twenty-first century simulation here (Fig. 1), allows a more energetic MJO-like signal in their aquaplanet simulation. Detailed budget analyses will be required to determine if similar processes will be in play for warmed future climate states.

## 5 Summary and discussion

The response of the MJO to climate change is studied using the CCSM4 model by comparing a current climate run to an extreme global warming scenario. Changes in the mean tropical climate support higher amplitude MJO events. Yet the MJO occurs less frequently in the warmer simulation. The MJO also tends to propagate further into the central and eastern Pacific in a warmer world. The number of MJO occurrences in the IO and western Hemisphere also increases by about 7 % in the future climate case, while the occurrence rate in the rest of the tropics increases to a lesser extent. The increase in average MJO amplitude and enhanced high amplitude MJO activity in the global warming scenario is consistent with previous studies showing extreme precipitation events amplifying in a warmer atmosphere (Allan and Soden 2008; O’Gorman and Schneider 2009b).

Previous observational studies indicate that the MJO shows regime changes on low-frequency time-scales (Jones and Carvalho 2011). Jones and Carvalho (2006) show a long-term trend in the MJO activity in reanalysis product including a trend toward greater event frequency after the mid-1970s (Jones and Carvalho 2006; Pohl and Matthews 2007). The changes in the MJO shown by these studies coincide with the long-term warming in the Indian Ocean and western Pacific warm pool.

The mechanisms involved in the initiation, propagation and non-periodicity of the MJO continue to present a major

challenge to develop a complete theory of the oscillation. Many previous studies have improved our understanding of the characteristics of the MJO changes due to background climate changes on seasonal to interannual time scales (Zhang 2005; Kiladis et al. 2009; Lau and Waliser 2012). In contrast, the behavior of the MJO on longer time scales is not clear, largely due to a lack of data records long enough to resolve interannual fluctuations of intraseasonal variability. Climate modeling studies and reanalysis products provide an important bridge to understanding these effects. Warmer tropical oceans causing increased MJO activity was shown by (Slingo et al. 1999) using controlled model experiments. Yet, there is a lack of sufficient understanding of dynamical mechanisms that explain this concurrent warming of the oceans and the concomitant increase in intraseasonal variability in the tropics. Low-level convergence of moist static energy and concurrent mid-tropospheric drying from a previous MJO cycle acts as precursors to the MJO initiation in the IO. Warmer Indian and Pacific oceans can increase the background convective available potential energy available for triggering MJO events.

The results from this study raise some important questions that deserve future investigation. Further studies with idealized GCMs and climate models are needed to clarify the dynamical mechanisms forcing regime changes in the MJO. Links between regime changes in the MJO and other low-frequency modes of the coupled ocean-atmosphere system (e.g., ENSO, the Indian Monsoon, Walker Cell, etc.; see Subramanian et al. 2011, for preliminary results) need to be investigated further. Since the MJO is a critical component in modulating weather variability in the tropics and extratropics of both hemispheres, knowledge of the long-term behavior of the MJO is very important in having a good understanding of future climate states and consequences for humanity.

**Acknowledgments** This research forms a part of the Ph.D. dissertation of A.S. We gratefully acknowledge funding from ONR (N00014-13-1-0139) and NSF (OCE-0960770). This research was initiated during a visit by A.S. to NCAR funded by the SUNNY (Scripps/UCSD/NCAR New and Young) Program. A.S. acknowledges NCARs computational support for simulations conducted for this study. We thank Mitch Moncrieff and Brian Mapes for erudite comments, and criticism of this work. A.S. extends heartfelt thanks to Bruce Cornuelle and Ian Eisenman for many invaluable gems of wisdom on science and data analysis. Part of this research was carried out at the Jet Propulsion Laboratory, California Institute of Technology, under a contract with the National Aeronautics and Space Administration.

## References

- Allan RP, Soden BJ (2008) Atmospheric warming and the amplification of precipitation extremes. *Science* 321:1481–1484
- Allen MR, Ingram WJ (2002) Constraints on future changes in climate and the hydrologic cycle. *Nature* 419:224–232
- D’Agostini G (2003) Bayesian reasoning in data analysis—a critical introduction. World Scientific, Singapore
- Deser C, Phillips AS, Tomas RA, Okumura YM, Alexander MA, Capotondi A, Scott JD, Kwon YO, Ohba M (2012) ENSO and Pacific decadal variability in the community climate system model version 4. *J Clim* 25:2622–2651
- Gent P, Yeager S, Neale RB, Levis S, Bailey D (2010) Improvements in a half degree atmosphere/land version of the CCSM. *Clim Dyn* 34:819–833
- Gent PR, Danabasoglu G, Donner LJ, Holland MM, Hunke EC, Jayne SR, Lawrence DM, Neale RB, Rasch PJ, Vertenstein M, Worley PH, Yang ZL, Zhang M (2011) The community climate system model version 4. *J Clim* 24:4973–4991
- Held IM, Soden B (2006) Robust responses of the hydrological cycle to global warming. *J Clim* 19:5686–5699
- Jochum M, Danabasoglu G, Holland M, Kwon Y, Large W (2008) Ocean viscosity and climate. *J Geophys Res* 113:C06017 doi:10.1029/2007JC004515
- Jones C, Carvalho L (2006) Changes in the activity of the Madden–Julian oscillation during 1958–2004. *J Clim* 19:6353–6370
- Jones C, Carvalho L (2011) Will global warming modify the activity of the Madden–Julian oscillation? *Q J R Meteorol Soc* 137:544–552
- Karnauskas KB, Seager R, Kaplan A, Kushnir Y, Cane MA (2009) Observed strengthening of the zonal sea surface temperature gradient across the equatorial Pacific Ocean\*. *J Clim* 22:4316–4321
- Kiladis GN, Wheeler M, Haertel P, Straub K, Roundy P (2009) Convectively coupled equatorial waves. *Rev Geophys* 47:RG2003 doi:10.1029/2008RG000266.
- Lamarque JF, Bond TC, Eyring V, Granier C, Heil A, Klimont Z, Lee D, Liousse C, Mieville A, Owen B, Schultz MG, Shindell D, Smith SJ, Stehfest E, Van Aardenne J, Cooper OR, Kainuma M, Mahowald N, McConnell JR, Naik V, Riahi K, van Vuuren DP (2010) Historical (1850–2000) gridded anthropogenic and biomass burning emissions of reactive gases and aerosols: methodology and application. *Atmos Chem Phys* 10:7017–7039
- Lamarque JF, Kyle GP, Meinshausen M, Riahi K, Smith SJ, van Vuuren DP, Conley AJ, Vitt F (2011) Global and regional evolution of short-lived radiatively-active gases and aerosols in the Representative Concentration pathways. *Clim Chang* 109:191–212
- Lau WK (2005) El Niño southern oscillation connection. In: *Intraseasonal variability in the atmosphere-ocean climate system*. Springer, Berlin, pp 271–305
- Lau WK, Waliser DE (2012) *Intraseasonal variability in the atmosphere-ocean climate system*. In: Springer-Praxis books. Springer, Berlin
- Lin J, Weickmann K, Kiladis G, Mapes B, Sperber K, Lin W, Wheeler M, Schubert S, Genio AD, Donner LJ, Emori S, Gueremy JF, Hourdin F, Rasch PJ, Roeckner E, Scinocca JF (2006) Tropical intraseasonal variability in 14 IPCC AR4 climate models. Part I: convective signals. *J Clim* 19:2665–2690
- Lin S (2004) A “vertically Lagrangian” finite-volume dynamical core for global models. *Mon Weather Rev* 132:2293–2307
- Liu P, Li T, Wang B, Zhang M, Luo JJ, Masumoto Y, Wang X, Roeckner E (2012) MJO change with A1B global warming estimated by the 40-km ECHAM5. *Clim Dyn*. doi:10.1007/s00382-012-1532-8
- Madden RA, Julian P (1994) Observations of the 40–50-day tropical oscillation—a review. *Mon Weather Rev* 122:814–837
- Maloney ED, Sobel AH, Hannah WM (2010) Intraseasonal variability in an aquaplanet general circulation model. *J Adv Model Earth Syst* 2. doi:10.3894/JAMES.2010.2.5

- Matthews A (2004) Variability of Antarctic circumpolar transport and the southern annular mode associated with the Madden–Julian oscillation. *Geophys Res Lett* 31:L24312. doi:[10.1029/2004GL021666](https://doi.org/10.1029/2004GL021666).
- Matthews A, Singhruck P, Heywood KJ (2007) Deep ocean impact of a Madden–Julian oscillation observed by Argo floats. *Science* 318:1765–1769
- McPhaden M (1999) Genesis and evolution of the 1997–1998 El Niño. *Science*. doi:[10.1126/science.283.5404.950](https://doi.org/10.1126/science.283.5404.950)
- Meehl GA, Washington WM, Arblaster JM, Hu A, Teng H, Tebaldi C, Sanderson BN, Lamarque JF, Conley A, Strand WG, White JB III (2012) Climate system response to external forcings and climate change projections in CCSM4. *J Clim* 25:3661–3683
- Moss RH, Edmonds JA, Hibbard KA, Manning MR, Rose SK, van Vuuren DP, Carter TR, Emori S, Kainuma M, Kram T, Meehl GA, Mitchell JFB, Nakicenovic N, Riahi K, Smith SJ, Stouffer RJ, Thomson AM, Weyant JP, Wilbanks TJ (2010) The next generation of scenarios for climate change research and assessment. *Nature* 463:747–756
- Neale R, Richter J, Jochum M (2008) The impact of convection on ENSO: from a delayed oscillator to a series of events. *J Clim* 21:5904–5924
- Neale RB, Richter J, Park S, Lauritzen PH, Vavrus SJ, Rasch PJ, Zhang M (2012) The mean climate of the community atmosphere model (CAM4). *J Clim*. doi:[10.1175/JCLI-D-12-00236.1](https://doi.org/10.1175/JCLI-D-12-00236.1)
- O’Gorman PA, Schneider T (2008) The hydrological cycle over a wide range of climates simulated with an idealized GCM. *J Clim* 21:3815–3832
- O’Gorman PA, Schneider T (2009a) Scaling of precipitation extremes over a wide range of climates simulated with an idealized GCM. *J Clim* 22:5676–5685
- O’Gorman PA, Schneider T (2009b) The physical basis for increases in precipitation extremes in simulations of 21st-century climate change. *Proc Natl Acad Sci* 106:14773–14777
- Pohl B, Matthews A (2007) Observed changes in the lifetime and amplitude of the Madden–Julian oscillation associated with interannual ENSO sea surface temperature anomalies. *J Clim* 20:2659–2674
- Richter J, Rasch PJ (2008) Effects of convective momentum transport on the atmospheric circulation in the community atmosphere model, version 3. *J Clim* 21:1487–1499
- Roundy PE, MacRitchie K, Asuma J, Melino T (2010) Modulation of the global atmospheric circulation by combined activity in the Madden–Julian oscillation and the El Niño–Southern oscillation during boreal winter. *J Clim* 23:4045–4059
- Schneider T, O’Gorman PA, Levine XJ (2010) Water vapor and the dynamics of climate changes. *Rev Geophys* 48:RG3001. doi:[10.1029/2009RG000302](https://doi.org/10.1029/2009RG000302)
- Seager R, Naik N, Vogel L (2012) Does global warming cause intensified interannual hydroclimate variability? *J Clim* 25:3355–3372
- Slingo JM, Rowell DP, Sperber KR, Nortley F (1999) On the predictability of the interannual behaviour of the Madden–Julian oscillation and its relationship with El Niño. *Quart J R Meteorol Soc* 125:583–609
- Stevenson S, Fox-Kemper B, Jochum M, Neale R, Deser C, Meehl G (2011) Will there be a significant change to El Niño in the 21st century? *J Clim* 25:2129–2145
- Subramanian AC, Jochum M, Miller A, Murtugudde R, Neale R, Waliser DE (2011) The Madden–Julian oscillation in CCSM4. *J Clim* 24:6261–6282
- Tokenaga H, Xie S-P, Deser C, Kosaka Y, Okumura YM (2012) Slowdown of the Walker circulation driven by tropical Indo-Pacific warming. *Nature* 491:439–443
- Trenberth K, Dai A, Rasmussen RM (2003) The changing character of precipitation. *Bull Am Meteorol Soc* 84:1205–1217
- Vecchi G, Soden B, Wittenberg A, Held IM (2006) Weakening of tropical Pacific atmospheric circulation due to anthropogenic forcing. *Nature* 441. doi:[10.1038/nature04744](https://doi.org/10.1038/nature04744)
- Waliser DE (2006) Intraseasonal variability. In: Wang B (ed) *The Asian monsoon*. Springer, Berlin, pp 203–257
- Waliser DE, Sperber K, Hendon HH, Kim D, Maloney E, Wheeler M, Weickmann K, Zhang C, Donner LJ, Gottschalck J (2008) MJO simulation diagnostics. *J Clim* 22:3006–3030
- Wheeler M, Hendon, HH (2004) An all-season real-time multivariate MJO index: development of an index for monitoring and prediction. *Mon Weather Rev* 132:1917–1932
- Zhang C (2005) Madden–Julian oscillation. *Rev Geophys* 43:1–36
- Zhang C, Gottschalck J (2002) SST Anomalies of ENSO and the Madden–Julian oscillation in the Equatorial Pacific\*. *J Clim* 15:2429–2445
- Zhou L, Neale RB, Jochum M, Murtugudde R (2012a) Improved Madden–Julian oscillations with improved physics: the impact of modified convection parameterizations. *J Clim* 25:1116–1136
- Zhou L, Sobel AH, Murtugudde R (2012b) Kinetic energy budget for the Madden–Julian oscillation in a multiscale framework. *J Clim* 25:5386–5403